SiO_2 and CaF_2 Behavior During Shielded Metal Arc Welding and Their Effect on Slag Detachability of the CaO-CaF_2-SiO_2 Type ENiCrFe-7-Covered Electrode

HUANG WANG, RENYAO QIN, and GUO HE

The metallurgical behavior during shielded metal arc welding (SMAW) and the slag detachability of the CaO-CaF_2-SiO_2 type ENiCrFe-7-covered electrodes was investigated. The results indicated that the slag detachability could be improved as the SiO_2 in the flux coatings decreased. When the SiO_2 in the flux coating was 10.9 pct, about 28.3 pct CaF_2 resulted in the best slag detachability. The CaF_2 and SiO_2 in the flux coating interacted during SMAW to form gaseous SiF_4 to be evacuated. In the reactions, one SiO_2 consumed two CaF_2, leading to the reduction of the ratio of CaF_2/SiO_2. After comparing the slag compositions, the best slag detachability was obtained at $CaO:CaF_2:SiO_2$ = 1.7:1.8:1, but the worst slag detachability appeared at $CaO:CaF_2:SiO_2$ = 1.3:0.9:1. The XRD analysis revealed that the oxides and fluorides in the slags preferred to gather together to form cuspidine and other complex phases. If the CaF_2 was dominant in the slags, they intended to form homogenous porous microstructures that were relatively strong and would most likely detach from the weld metal in blocks, exhibiting good slag detachability. If the cuspidine phase was dominant, the slags exhibited a 'rock strata'-like microstructure in the intergranular area. Such microstructure was very fragile and could be broken into fine powders that were easily embedded in the weld ripples, leading to slag adhesions. This work provides the researcher with a wealth of information and data, which will also be beneficial to the welding material producers and users.

DOI: 10.1007/s11661-016-3629-x

I. INTRODUCTION

NICKEL-BASE alloys are very important engineering materials that can be used in a wide range of environments and applications due to their high resistance to the aqueous and high-temperature corrosion in complex atmospheres, and their high strength over a large temperature range from cryogenic up to high temperatures.[1] The Ni-base alloy welding consumables also can be used for welding the structures that serves in various harsh environments, because their weld metals can always maintain strength and ductility in a large temperature interval, despite significant dilution by other alloying elements.[1,2] ENiCrFe-7 is a typical nickel-base alloy covered electrode, which was recommended to be used for welding Inconel 690 and other similar applications to produce excellent as-welded strength and impact toughness and good corrosion resistance.[2,3] In welding practice, the covered electrodes (conforming to AWS A5.11/A5.11M ENiCrFe-7 specification) manufactured by different producers may exhibit very different weldability and operability including arc stability, weld contour, slag detachability, spatter and fume, *etc*. This is because different flux formulations have been used in each factory. Generally, the acidic flux system provides very good welding operability but relatively high-cracking susceptibility; while the basic flux system results in lower hydrogen in the weld metal but unfavorable welding operability.[4,5] For the nuclear power applications, low hydrogen and low cracking susceptibility are extremely important, so that the basic flux system should be the first choice. However, the welding operability becomes the main problem in this case. One of the concerns is poor slag detachability that seriously affects productivity.

It has already been recognized that the slag detachability has very close relations with both the physical and chemical properties of the flux.[4–7] One of the mechanism of slag adhesion to weld metal is the chemical bond *via* forming a thin layer of oxides of elements of the metal phase on the weld metal surface.[6] This chemical bond can be eased or eliminated if a slag system with the minimal oxidizing ability was used (*e.g*., basic flux system).[4–6] The other factors affecting the slag detachability are the differences between the thermal expansion coefficients of the slag and the weld metal, and the phase transformations in the slag during

HUANG WANG and RENYAO QIN, Ph.D. Students, are with the Shanghai Key Laboratory of Materials Laser Processing and Modification and State Key Laboratory of Metal Matrix Composites, School of Materials Science and Engineering, Shanghai Jiao Tong University, Shanghai 200240, China. GUO HE, Professor, is with Shanghai Key Laboratory of Materials Laser Processing and Modification and State Key Laboratory of Metal Matrix Composites, School of Materials Science and Engineering, and also with the Collaborative Innovation Center for Advanced Ship and Deep-Sea Exploration, Shanghai 200240, China. Contact e-mail: ghe@sjtu.edu.cn

Manuscript submitted November 23, 2014.
Article published online July 8, 2016

cooling.[4,7] An appropriate thermal expansion difference is necessary for good slag detachability, but too early slag detachment should be avoided so as to prevent undesired heavy temper colors.[8] Some experiments on the mild steel electrode coatings suggested that slags containing [Cr, Mn, Mg]O, [Cr, Mn, Al]$_2O_3$ type spinels, or cordierite ($Mg_2Al_4Si_5O_{18}$) glass structure, or $(CaO)_2SiO_2$, Cr_2TiO_5, and $FeTiO_5$ phases generally have poor slag detachability.[4,9] The CaO-CaF_2-SiO_2 and CaO-TiO_2-SiO_2 flux systems were considered to have acceptable slag detachability.[9] Rutile in the flux generally improves slag detachability, but fluorite affects in opposite manner.[6–10] Increasing the Al_2O_3 content in the flux is helpful for the slag detachability.[4] However, these univariate regularities are only valid under certain respective conditions. We have found in practice that cryolite can also improve slag detachability in the acidic flux system, but worsen the slag detachability in the basic flux system of the ENiCrFe-7. The rutile may cause poor slag detachability if its content was larger than 5 pct in the basic flux system of the nickel-base alloy covered electrodes, such as ENiCrFe-7 and ENiCrFe-3. Fluorite improves the slag detachability in the basic flux system of the ENiCrFe-7, but does not in the acidic flux system.

Other than the flux ingredients mentioned above, silica should also be noted which is usually used in the flux coating of the carbon steel electrodes partially instead of rutile, but is not used in the stainless steel and nickel-base alloy covered electrodes because it can cause serious slag adhesion. In spite of this, the silicon dioxide can be one of the main components in the CaO-CaF_2-SiO_2 flux system of the ENiCrFe-7 electrode.[11] It was introduced from the binder in the flux coating (*i.e.*, sodium silicate) and the deoxidizer (*i.e.*, ferrosilicon). By carefully distinguishing the silicon dioxide in the slag, we found that different fractions of the silicon dioxide in the slag correspond to dispersed slag detachability; one could not establish a relationship between the silicon dioxide content and the slag detachability. However, when considering the cross effect of various oxides, one could easily establish a relationship between the ratio of CaF_2 to SiO_2 and the slag detachability. In this paper, we report the detail of this finding. The possible metallurgical chemical mechanism will be discussed based on the experimental results.

II. EXPERIMENTAL PROCEDURE

The nickel-base alloy ENiCrFe-7 covered electrode with CaO-CaF_2-SiO_2 type flux coating has been developed in our laboratory, which has desirable operability and good weldability. In order to investigate the slag detachability, two groups of flux formulations were specially designed for revealing the influence of the SiO_2 and CaF_2 in the flux, which were listed in Table I (A-group: SiO_2 is the variable quantity, and B-group: CaF_2 is the variable quantity). Apart from the three main ingredients, other additives listed in Table I were employed for achieving better performance of welding process and providing specified composition in the deposited metal (25 pct Na_2O + 75 pct SiO_2: a major constituent of sodium silicate, used as binder and arc stabilizer; Na_2CO_3: for improving the manufacturability of the covered electrodes; 45 pct Si + 55 pct Fe and 28 pct Ti + 72 pct Fe: both are strong deoxidizers; Mn, Cr and 50 pct Nb + 50 pct Fe: alloying elements). In experiment, the weight percentages of each ingredient were transformed into that of the commercial minerals, such as marble, fluorite, and silica, according to their actual compositions in the minerals. All the minerals and metal powders used were controlled in the range of 100 to 250 μm in particle size. The minerals were first mixed uniformly with the metal powders and were bonded with water glass. Then the covered electrodes were produced in the lab with the standard processing technique that was commonly used in the welding material factory. The nickel-base alloy core wire with dimension of Φ3.2 mm × 350 mm was manufactured in our partner factory. Its chemical composition was reinspected and listed in Table II.

The welding operation was performed on a carbon steel plate with DC reverse polarity. The welding current was 110A; the arc voltage was 23 to 25 V; the welding velocity was 3.5 to 4.0 mm/s. The heat input was 0.63 to 0.79 KJ/mm. After welding, the steel plate was gently knocked three times. If all the slag was detached, the slag detachability is the best. Otherwise, if the slag was partially detached and some slag still stuck on the weld metal, the slag detachability is not so good. For quantitatively measuring the slag detachability, the images of the weld seam with the residual slag were analyzed using the commercial Image-Pro Plus software

Table I. The Designed Flux Formulations of the Nickel-Base Alloy Covered Electrodes (Weight Percent)

Groups	No.	$CaCO_3$	CaF_2	SiO_2	25 pct Na_2O + 75 pct SiO_2	45 Pct Si + 55 Pct Fe	28 Pct Ti + 72 Pct Fe	50 Pct Nb + 50 Pct Fe	Na_2CO_3	Mn	Cr
A	A1	43.8	21.9	—	9.6	3.8	4.9	3.3	0.6	8.8	3.3
	A2	41.5	20.8	**5.2**	9.1	3.6	4.7	3.1	0.5	8.3	3.1
	A3	39.5	19.7	**9.9**	8.7	3.5	4.4	3.0	0.5	7.9	3.0
B	B1	41.5	**20.8**	5.2	9.1	3.6	4.7	3.1	0.5	8.3	3.1
	B2	39.5	**24.7**	4.9	8.7	3.5	4.4	3.0	0.5	7.9	3.0
	B3	37.6	**28.3**	4.7	8.3	3.3	4.2	2.8	0.5	7.5	2.8
	B4	35.9	**31.5**	4.5	7.9	3.1	4.0	2.7	0.5	7.2	2.7
	B5	34.3	**34.3**	4.3	7.6	3.0	3.9	2.6	0.4	6.9	2.6

The bold values are indication that they are the design variables.

Table II. Chemical Composition of the Core Wire (Weight Percent)

C	Si	Mn	S	P	Fe	Nb	Cr	Ni
0.025	0.11	0.90	0.005	0.015	4.40	2.10	29.20	balance

to determine the relative fraction of the slag adhesion area. Then the 'slag removal fraction,' SRF, could be defined as

$$\mathrm{SRF} = \frac{A_0 - A_s}{A_0} \times 100 \text{ pct}, \quad [1]$$

where A_0 indicates the total area of the weld seam in the image; A_s indicates the slag adhesion area.

In addition, the bulk slag was directly observed and analyzed under the FEI QUANTA 250 scanning electron microscope (SEM) with Oxford energy dispersive spectrometer (EDS) to determine the local compositions and oxide phases. The average compositions of the slag were analyzed using the Thermo Fisher ARL9900 X-ray fluorescence spectrometer (XRF). Before the analysis, the bulk slag was crushed and ground into about 200 mesh powder. The metals and other main elements such as fluorine, silicon, and calcium in the slag could be quantitatively identified by the XRF analysis. Considering that the slag consists of oxides and fluoride,[12] the overall slag composition could be expressed in terms of calcium fluoride and stoichiometric basic and acidic oxides. Besides, the fine slag powders were also used for the X-ray diffraction (XRD) analysis to determine the main phases in the slag. The XRD was performed using a Rigaku UItima IV X-ray diffractometer with CuKα radiation.

III. RESULTS

A. *Observations on the Welding Slag*

The ENiCrFe-7-covered electrodes with various flux coatings (as listed in Table I) exhibited different welding features, especially the behavior of the molten slags and the detachability of the solidified slags. For A-group, the fluidity of the molten slags became worse as the silicon oxide increased in the flux coating, but they all exhibited the similar slag coverage. The appearance of the weld beads before and after removal of the covered slags is shown in Figure 1. It was very distinct that as the SiO_2 increased (from A1 to A3), the color of the covered slags changed from dark blue (A1) to deep brown (A2) and then light brown (A3); the weld surface changed from fine to coarse ripples (the right half of Figure 1); and the slag detachability became worse. It should be also pointed out that the slag with dark blue color (Figure 1a) tended to detach in large chunks from the weld metal, but the brown slags were most likely broken into small pieces when knocking the weld bead, and left some slag powders adhered on the surface of the weld metal as shown in Figures 1(b) and (c). The observation on the broken slags confirmed that the A1 slag was very dense, and there was no visible pore under the macroscopic views (Figure 2(a)). However, the A2 and A3 slags showed obvious porosity (Figures 2(b) and (c)), and the A3 slag was almost porous in whole. These observations suggested that the slag detachability became worse as the porosity increased in the slags.

Although the weight percentages of the CaF_2 in flux coatings changed in a large scale in B-group, the similar two kinds of the slags were also observed, *i.e.*, dark blue slag (B3) and brown slags (B1 and B2: deep brown; B4 and B5: brown) as shown in Figure 3. The slag with dark blue color (Figure 3(b)) exhibited the best slag detachability and also had good slag coverage and better welding operability during shielded metal arc welding (SMAW). The slags with brown color (Figures 3(a), (c), and (d)) brought about evident slag adhesion. When looked at the internal surface of the slags, the porosity could be also observed as shown in Figures 4(a), (c), and (d), which corresponded to B2, B4, and B5 slags. However, the B3 slag looked dense, and there was no visible porosity as shown in Figure 4(b). These observations also suggested that the porous slags were most easily adhered to the weld metal.

Based on the observations on the welds of A and B-groups, a relationship between the slag feature (*i.e.*, color and porosity) and the slag detachability could be established for this ENiCrFe-7 covered electrode, that is, the dark blue slag corresponded to the good slag detachability; as the slag color changed from dark blue to deep brown and light brown, the slag detachability tended to deteriorate. The dense slag led to relatively good slag detachability, but the porous slags resulted in poor slag detachability.

B. *SiO_2 and CaF_2 Behavior During Shielded Metal Arc Welding*

CaF_2 and SiO_2 are very important ingredients in both the flux coating and the slag. They, together with CaO, constitute a fundamental CaO-CaF_2-SiO_2 type slag system. Since the flux formulations contained many alloys that would be mostly transferred into the weld pool, there was no sense of comparison of the weight percentages of CaF_2 and SiO_2 between in the designed formulations and in the slags. However, the relative ratio of CaF_2 to SiO_2 indirectly implied their behavior and interaction during SMAW and then prompted us their influence on the welding operability, especially the slag detachability. To this end, all slags (corresponding to the two groups of the designed flux formulations, as listed in Table I) were analyzed and listed in Table III. Almost all the slags contained the three main components: CaO, CaF_2, and SiO_2, that accounted for about 80 to 85 pct of the total weights of the slags, while the other 15 to 20 pct of the slags were Na_2O, MnO, Cr_2O_3, Nb_2O_5, TiO_2, *etc.*, as indicated in Table III. By carefully comparing the three main components, one could find that the CaF_2 and SiO_2 exhibited obvious changing

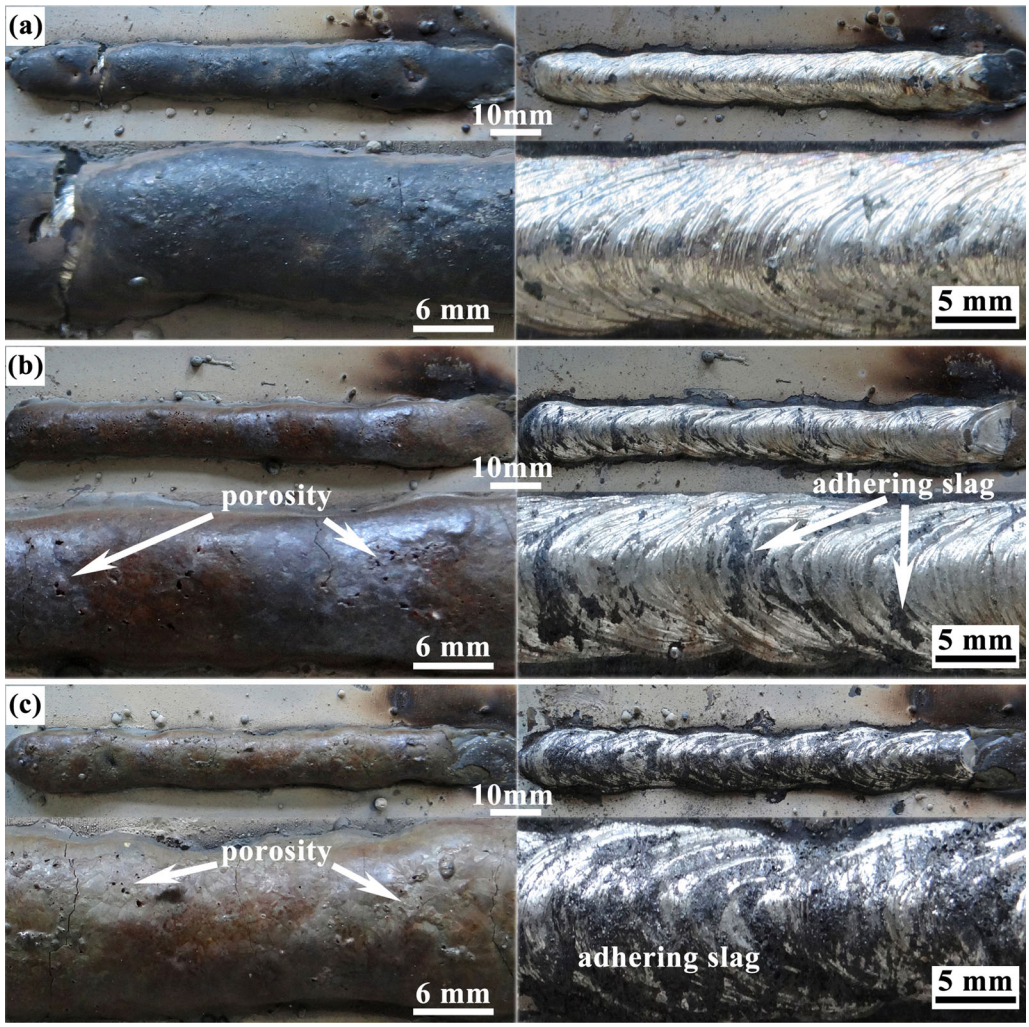

Fig. 1—Weld images of the ENiCrFe-7-covered electrodes with A-group flux coatings. (*a*) A1, (*b*) A2, and (*c*) A3. The left: the welds covered by slags; the right: the welds after removal of the slags.

trends and correlations in their compositions, *i.e.*, CaF_2 decreased significantly in the slag (A1–A3 in Table III) as the SiO_2 increased in the flux (A-group in Table I), while the SiO_2 firstly decreased and then became uncertain in the slag (B1–B5 in Table III) as the CaF_2 increased in the flux (B-group in Table I). It seemed that the CaF_2 and SiO_2 had strong interaction during SMAW, that is, the SiO_2 in the flux could consume the CaF_2 markedly during SMAW (A1–A3 in Table III, SiO_2 is the univariate quantity), but not *vice versa*, the CaF_2 in the flux did not reduce SiO_2 evidently (B1–B5 in Table III, CaF_2 is the univariate quantity). Besides, the CaO compositions seemed have no certain correlations to that of the CaF_2 and SiO_2 (A,B-groups in Table III).

Considering that the Si in the flux was partially transferred into the weld metal during SMAW,[11] the real amount of the Si in the slag must be less than that in the flux. For similar reason, the real amount of the CaF_2 in the slag must be less than that in the flux due to the F-consuming during SMAW (its mechanism will be discussed in the Section IV). In order to measure the behaviors of the CaF_2 and SiO_2, their relative ratios in both the flux formulations and the slags were calculated and listed together in Table IV. It was very obvious that all the ratios of CaF_2 to SiO_2 in the slags were smaller than that in the flux coatings for whether A-group or B-group, suggesting that the consumption of fluorine was more than that of Si during SMAW. This could be illustrated graphically by drawing the ratio lines in the SiO_2-CaF_2 coordinates, as shown in Figure 5. All the CaF_2/SiO_2 ratios of the slags fell under their respective ratio lines that were designed in their flux formulations.

C. *Effect of SiO_2 and CaF_2 in the Flux Coatings on the Slag Detachability*

Since the SiO_2 was the univariate quantity in A-group, its effect on the slag detachability could be shown in Figure 6(a). The SRF decreased sharply from 95 pct to about 42 pct as the silica in the flux coating increased from about 10 pct to about 19.7 pct (all the silicon inside the

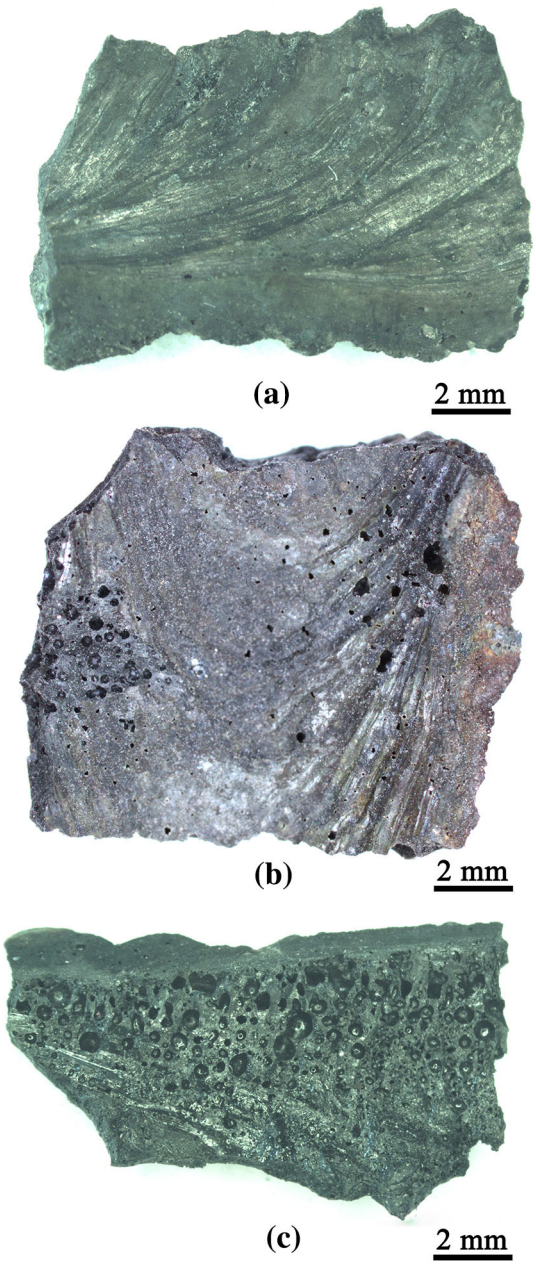

Fig. 2—The internal surface images of the slags of the ENiCrFe-7 covered electrodes. (*a*) A1, (*b*) A2, and (*c*) A3.

water glass and the ferrosilicon was included). In B-group (Table I), the tested data demonstrated an optimal composition value of the CaF_2 (about 28 pct in the flux coating), with which the SRF reached 100 pct as shown in Figure 6(b). If the complex effect of the SiO_2 and CaF_2 was considered, the SRF against the ratios of SiO_2/CaF_2 in the flux coatings was plotted in Figure 6(c). The SRF increased monotonically with increasing the ratio of SiO_2/CaF_2 from 1 to about 2 for either A-group or B-group. But further increasing the ratio led to decrease of the SRF value (for B-group). There was a maximal SRF value ($SiO_2/CaF_2 = 2.0$) in the investigated range of the ratios, with which the flux coating exhibited the best slag detachability (B3 in Tables I and IV).

D. *Characterization of Slags and Their Effect on the Slag Detachability*

To explore the slag detachability, the slag itself must be examined. The slags of A-group ENiCrFe-7 covered electrodes were carefully investigated using SEM, XRD, and EDS. Very different microstructures among the three kinds of the slags were observed as shown in Figure 7. A1 slag exhibited a homogenous porous microstructure (Figures 7(a) and (b)) in which the solid phases with size of about 10 to 40 μm interconnected each other, while the pores with size of below about 10 μm dispersed among the solid phases. Under larger magnification, the solid phases were revealed which were the fused mixtures of a large number of small particles as shown in Figure 7(c). The EDS results (Table V) indicated that the solid phase was a mixture of oxides and fluorides. Particularly, the oxides were the dominant components for the c1 and c3 particles and c4 area, but the fluorides were the dominant components for c2 particle as marked in Figure 7(c). It should be specially noted that the interconnection of these solid phases were relatively strong, so the A1 slag most likely detached from the weld metal in blocks.

Unlikely, A2 slag exhibited a relatively coarse microstructure where the massive phases with size of about 40 to 100 μm were stacked together (Figures 7(d) and (e)). The boundary between the massive phases was filled with separate crystals that have specific faceted features as shown in Figure 7(f). It was very palpable that the massive phase was relatively dense, but the boundary microstructure was composed of various crystals that grew up, respectively, during solidification of the slag (Figure 7(f)). Since the melt/crystal transformation in the boundary area occurred in the final solidification stage, the solidification shrinkage cannot be compensated for, leading to porous boundary microstructure. With such boundary morphology, the slag was expected to be brittle and weak. Referring to the EDS results (Table V), one could easily find out that the massive phases were mainly composed of Ca-Si-O-F compounds (phases e1 and e2 as listed in Table V and shown in Figure 7(e)) that had relatively higher melting points. The boundary phases (faceted crystals) could be at least classified into four kinds of compounds (phases f1–f4 as listed in Table V and shown in Figure 7(f)) that had relatively lower melting points. The calcium and silicon oxides were dominant in f2 crystal, but the calcium fluorides were dominant in f3 crystal (Table V; Figure 7(f)). It was interesting to find that the chromium oxide-rich compound (f1) and the sodium and niobium oxides-bearing compound (f4) existed in the boundary microstructure.

A3 slag exhibited the coarsest microstructure in which the dense particles (massive phases) with size of about 100 to 300 μm were embedded in a white matrix as shown in Figure 7(g). Under larger magnification (Figure 7(h)), the white matrix had a porous microstructure in which many 'blocks' (a faceted phase) stacked together forming such 'rock strata'-like microstructure (Figure 7(i)). The EDS analysis indicated that its composition was similar to that of f2 crystal (Figure 7(f);

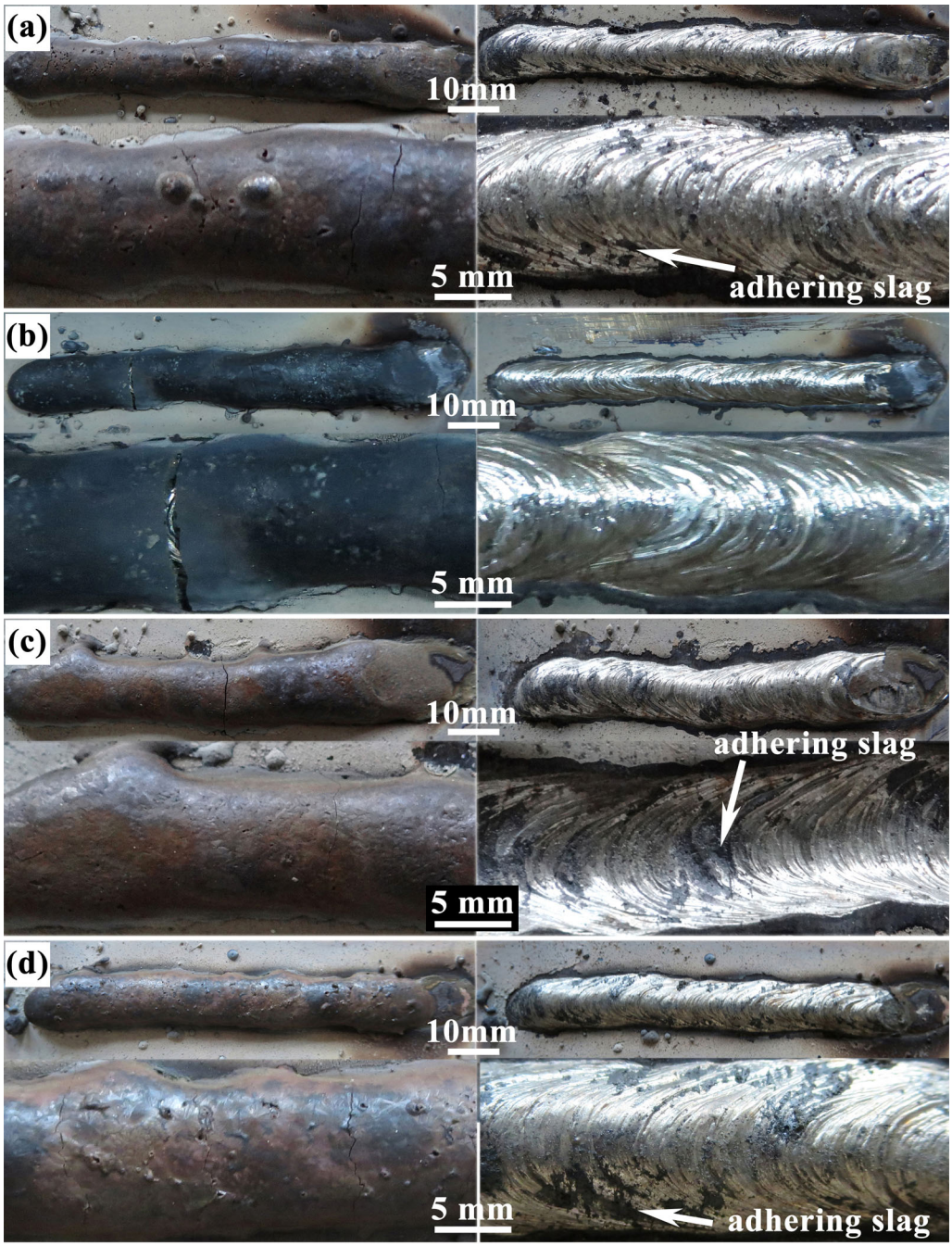

Fig. 3—Weld images of the ENiCrFe-7-covered electrodes with B-group flux coatings. (*a*) B2, (*b*) B3, (*c*) B4, and (*d*) B5. The left: the welds covered by slags; the right: the welds after removal of the slags.

Table V), suggesting a Ca-Si-O-F compound with more oxides but less fluorides. Such 'rock strata'-like microstructure was generally brittle.

XRD analysis indicated that all the slags (A1–A3) were composed of CaF_2 [T_m = 1703 K (T_m = 1430 °C)[13]] and cuspidine [$3CaO{\cdot}2SiO_2{\cdot}CaF_2$, T_m = 1680 K (T_m = 1407 °C)[14]] phases, as well as the high melting point phases ($2CaO{\cdot}SiO_2$, T_m = 2403 K (T_m = 2130 °C);[15] and $3CaO{\cdot}SiO_2$, T_m = 2343 K (T_m = 2070 °C)[15]) as shown in Figure 8. However, the CaF_2 was dominant in A1 slag, but the cuspidine phase was dominant in both A2 and A3 slags, suggesting that A1 slag contained more CaF_2, but A2 and A3 slags contained relative low CaF_2. This was in good agreement with the average composition of the slags determined by XRF analysis as listed in Table III.

Although the oxides and fluorides in the slags preferred to assemble together to form cuspidine and high melting point $2CaO{\cdot}SiO_2$ and $3CaO{\cdot}SiO_2$ phases, it

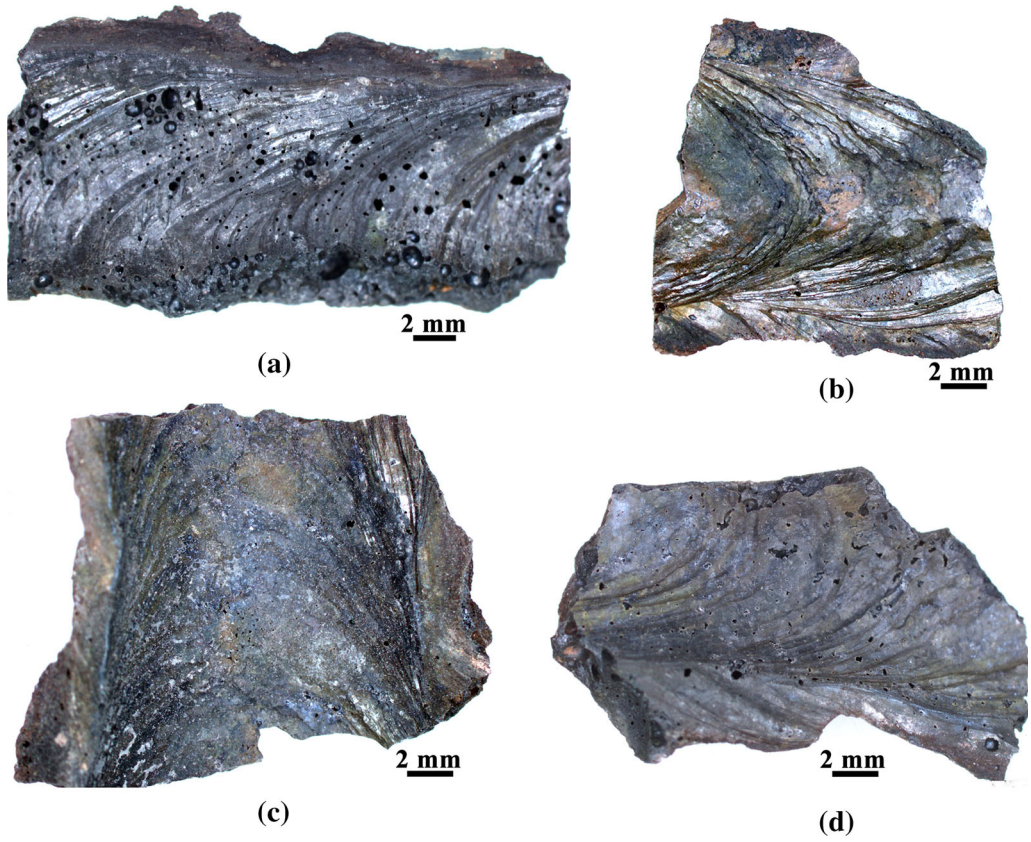

Fig. 4—The internal surface images of the slags of the ENiCrFe-7-covered electrodes. (*a*) B2, (*b*) B3, (*c*) B4, and (*d*) B5.

Table III. Compositions of the Welding Slags of the Covered Electrodes (Weight Percent)

No.	CaO	CaF_2	SiO_2	Na_2O	MnO	Cr_2O_3	Nb_2O_5	TiO_2	Al_2O_3	FeO	K_2O	NiO	MgO
A1	31.89	31.30	17.81	3.52	3.34	2.81	2.98	3.40	1.18	0.50	0.38	0.26	0.31
A2	32.60	24.29	21.79	3.74	4.23	3.97	3.26	3.09	1.20	0.48	0.34	0.36	0.28
A3	31.76	21.78	24.60	3.39	5.05	4.69	2.96	3.10	1.15	0.41	0.36	0.33	0.30
B1	32.60	24.29	21.79	3.74	4.23	3.97	3.26	3.09	1.20	0.48	0.34	0.36	0.28
B2	30.10	31.00	21.00	3.66	2.80	3.06	2.71	2.94	1.20	0.46	0.33	0.31	0.27
B3	32.10	33.60	18.65	3.52	2.47	2.30	2.60	2.88	1.16	0.47	0.30	0.42	0.25
B4	26.95	34.56	20.17	3.79	3.30	3.37	2.58	2.87	1.17	0.46	0.36	0.29	0.20
B5	24.90	38.88	18.75	3.59	3.05	3.35	2.47	2.44	1.00	0.41	0.35	0.26	0.22

Table IV. Percentages of the Three Main Ingredients in Both the Designed Flux Formulations and the Slags (Weight Percent)

	Designed Flux Formulations					Slags						
No.	$CaCO_3$	CaF_2	SiO_2	Si*	CaF_2:SiO_2	CaO	CaF_2	SiO_2	CaF_2:SiO_2	CaO:CaF_2:SiO_2	(CaO + CaF_2):SiO_2	SRF (pct)
A1	43.8	21.9	7.2	1.7	2.0	31.89	31.30	17.81	1.8	1.8:1.8:1	3.55	95.0
A2	41.5	20.8	12.0	1.6	1.4	32.60	24.29	21.79	1.1	1.5:1.1:1	2.61	70.5
A3	39.5	19.7	16.4	1.5	1.0	31.76	21.78	24.60	0.9	1.3:0.9:1	2.18	42.5
B1	41.5	20.8	12.0	1.6	1.4	32.60	24.29	21.79	1.1	1.5:1.1:1	2.61	70.5
B2	39.5	24.7	11.5	1.5	1.7	30.10	31.00	21.00	1.5	1.4:1.5:1	2.91	75.1
B3	37.6	28.3	10.9	1.5	2.0	32.10	33.60	18.65	1.8	1.7:1.8:1	3.52	100
B4	35.9	31.5	10.4	1.4	2.4	26.95	34.56	20.17	1.7	1.3:1.7:1	3.05	79.3
B5	34.3	34.3	10.0	1.4	2.6	24.90	38.88	18.75	2.1	1.3:2.1:1	3.40	81.5

* When calculating CaF_2:SiO_2, the Si percentages in the flux coatings were transferred into that of the SiO_2.

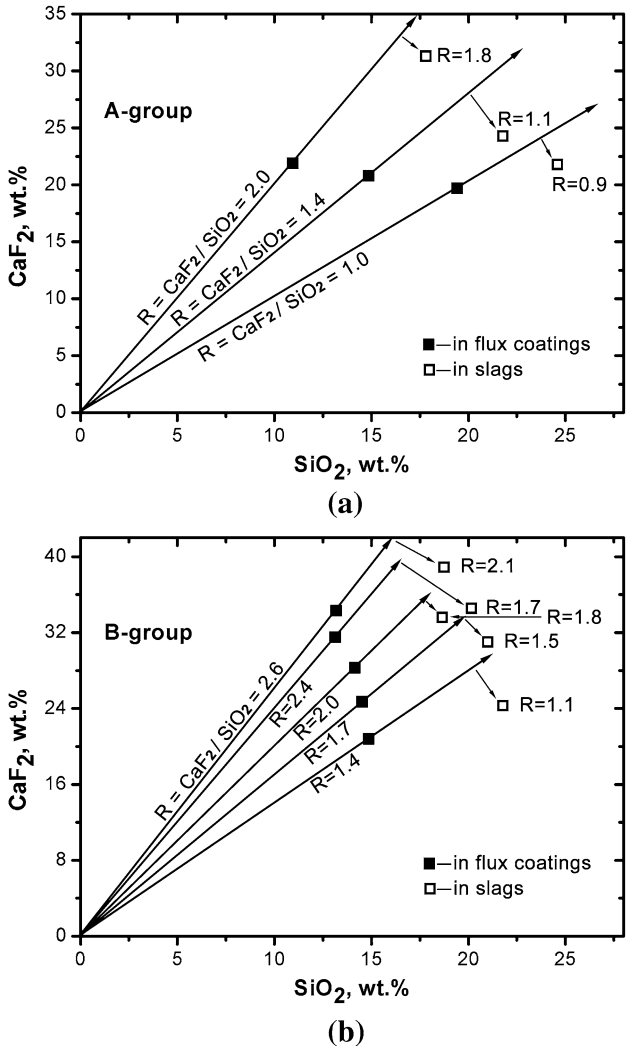

Fig. 5—Comparison of the CaF_2/SiO_2 ratios between in the flux coatings and in the slags. (*a*) for A-group and (*b*) for B-group.

is hard to quantitatively distinguish these compounds. Therefore, only the simple oxides and fluorides were considered when relating the slag composition to the slag detachability. As stated above, the slags were composed of about 80 to 85 pct CaO, CaF_2, and SiO_2. It was reasonable to believe that the correlations among the three main components must affect the slag detachability. Thus, the relative weight ratios of CaO, CaF_2 and SiO_2, together with the ratios of $(CaO + CaF_2)/SiO_2$, were calculated and listed in Table IV. It was found that when $CaO:CaF_2:SiO_2$ = 1.7:1.8:1 (B3) or 1.8:1.8:1 (A1), the slag detachability was very good, but when $CaO:CaF_2:SiO_2$ = 1.3:0.9:1 (A3), it became the worst. If considering $(CaO + CaF_2)/SiO_2$ only, the slag detachability became better as the ratio increased from 2.18 to 3.52. Further increasing the ratio led to the deterioration of the slag detachability. There was an optimal $(CaO + CaF_2)/SiO_2$ (equal to about 3.5) that provided the best slag detachability as shown in Figure 9.

IV. DISCUSSION

A. *SiO_2 and CaF_2 Behavior and Interaction During Shielded Metal Arc Welding*

The SiO_2 in the slags came from the sodium silicate, ferrosilicon, and silica used in the flux coatings. The CaF_2 in the slags came from the fluorite in the flux coatings. Another main component, CaO, in the slags was produced from the decomposition of the marble at arc temperature, which has been widely used in various types of fluxes. These three main components constituted the fundamental $CaO-CaF_2-SiO_2$ slag system. The purpose and functions of each component have been generally explained in the literatures.[4–10] For example, all the three are deoxidizers and can be used to control the viscosity of the molten slag; d both CaO and SiO_2 are arc stabilizers, but CaF_2 can provide gaseous protection.[4,5] Other than those, the CaO can act as a melt purification agent for desulfurization and dephosphorization by following reactions:[16,17]

$$FeS + CaO \rightarrow CaS + FeO \quad [2]$$

$$P_2O_5 + 3CaO \rightarrow Ca_3P_2O_8 \quad [3]$$

It can also restrain the decomposition reaction of SiO_2, reducing the Si mass transfer from the flux coating to the melt pool, because the strong basic CaO chemically balances the strong acidic SiO_2.[18] However, all these reactions do not significantly reduce the amount of the CaO in the slag, but may slightly affect the amount of SiO_2 in the slag. These chemical metallurgical effects are consistent with the measurements on A and B-group slags as listed in Table III.

The SiO_2 in the slags must be less than that in the flux coatings because the Si was partially consumed during SMAW in two ways: (1) transferred into the weld metal and (2) reacted with CaF_2 to form gaseous SiF_4 to be evacuated. For the $CaO-CaF_2-SiO_2$ type ENiCrFe-7 covered electrodes, the Si mass transfer coefficient was reported in the range of 41 to 47 pct,[11] suggesting that the Si transfer from the flux coating into the weld metal was significant. The SiO_2-consuming by CaF_2 depended on the absolute amount of the CaF_2 in the flux coating. The higher content of the CaF_2 generally consumed more SiO_2 during SMAW according to the following formula:

$$2CaF_2 + SiO_2 \rightarrow SiF_4 \uparrow + 2CaO \quad [4]$$

It was clear that one SiO_2 consumed two CaF_2, but produced two CaO. This suggests that the absolute amounts of both the CaF_2 and SiO_2 in the flux coating were reduced after SMAW, and the reduction of the CaF_2 was larger than that of the SiO_2, completely consistent with the experimental results as shown in Figure 5.

In addition, the CaF_2 could also be consumed by crystal water in the minerals or by moisture pickup from the air at the arc temperature according to the following reaction:

$$CaF_2 + H_2O \rightarrow CaO + 2HF \uparrow \quad [5]$$

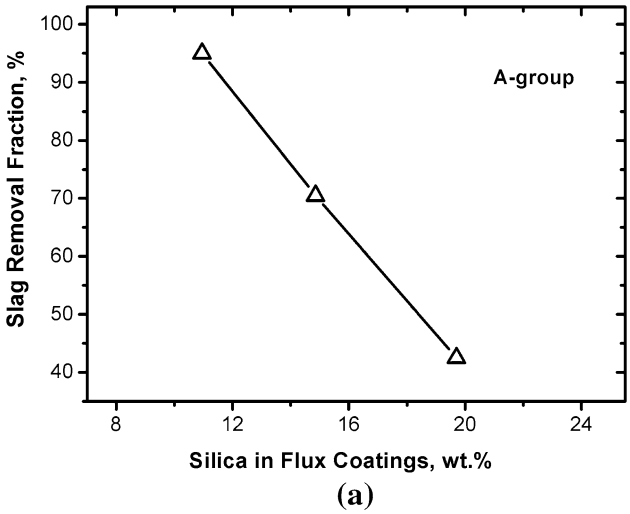

(a)

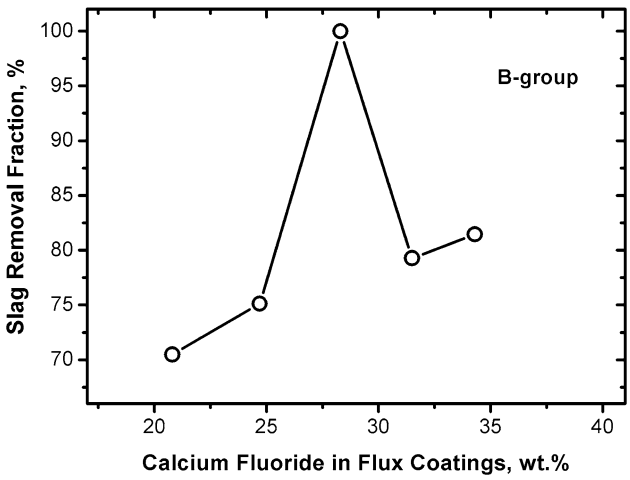

(b)

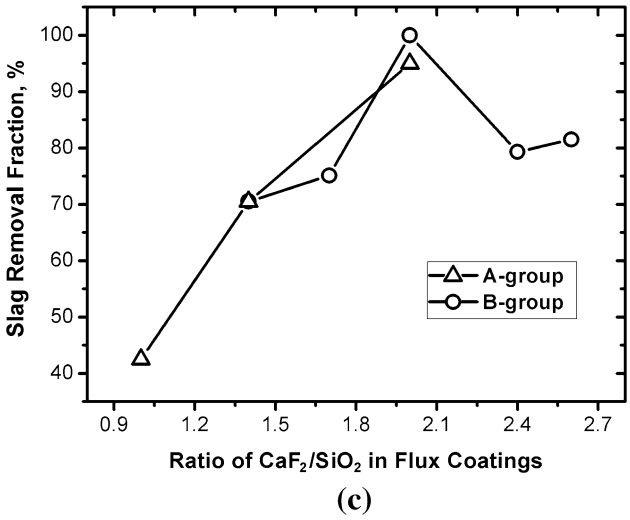

(c)

Fig. 6—Effect of the ingredients in the flux coatings on the slag removal fractions.

In summary, the three main components: CaO ($CaCO_3$), CaF_2, and SiO_2, in the flux coatings exhibited different behaviors during SMAW. The CaO decomposed from the $CaCO_3$ was kept at a relatively constant amount and would almost all be transferred into the slag, because it could not only be consumed by the desulfurization and dephosphorization reactions (Eqs. [2] and [3]), but also be generated by the CaF_2-consuming reactions (Eqs. [4] and [5]). Both the CaF_2 and SiO_2 would be partially consumed by either their interaction (Eq. [4]) or respective reactions (Eq. [5] and the decomposition of SiO_2 that led to Si transfer into weld metal[11]). Thus, the CaF_2 and SiO_2 in the flux coating were only partially transferred into the slags.

B. *Slag Detachability of the CaO-CaF_2-SiO_2 Type ENiCrFe-7 Covered Electrode*

The slag detachability depends on the weld metal/slag interface and the difference in the thermophysical properties between the metal and the slag. Generally, a distinct metal/slag interface corresponds to good slag detachability, otherwise, a blurred interface undoubtedly corresponds to poor slag detachability. In order to observe the morphology of the weld metal/slag interface, the weld bead covered by the slag was mounted by resin and then sectioned. It obviously revealed that the metal/slag interface had a zigzag pattern as shown in Figure 10. Under larger magnification, one could find that there was no distinct metal/slag boundary (Figure 10(c)), suggesting the possible chemical bond that was formed by oxidation of elements of the weld metal on the weld bead surface.[6] It was known that the chemical bond could be formed if a slag system with the high oxidizing ability was used.[4–6] As the slag basicity increased, the oxidizing ability of the slag decreased. Since the CaO and CaF_2 are typical alkaline compounds, and the SiO_2 is a strong acidic oxide, the ratios of the $(CaO + CaF_2)/SiO_2$ directly indicate the basicity index. Therefore, as the $(CaO + CaF_2)/SiO_2$ increased, the oxidizing ability of the slag decreased, *i.e.*, the tendency to form the chemical bond decreased (slag detachability increased). Such explanation was supported by the experimental results in this work as shown in Figures 9 and 10.

When evaluating the thermophysical properties of the three main components in the slags, one can rank the thermal expansion coefficients in the sequence of $CaF_2 > CaO > SiO_2$.[19–23] If simply considering the CaO-CaF_2-SiO_2 ternary system, the slags with more CaF_2 should have relatively larger thermal expansion coefficients. Conversely, the slags with more SiO_2 should have relatively smaller thermal expansion coefficients. Since the weld metal (in accord with Inconel 690) has the thermal expansion coefficient in the range of 13.5 to 17.6 $\times 10^{-6}$/°C at the temperature range of 366 K to 1255 K (93 °C to 982 °C),[19] which is close to that of the CaO.[20,21] It could be expected that the thermal expansion coefficient of the slags with more CaF_2 (*e.g.*, A1, B3, and B5) would be larger than that of the weld metal, while the slags with more SiO_2 (*e.g.*, A3 and A2) would have smaller thermal expansion coefficients than the weld metal. The slags with larger thermal expansion coefficients (A1 and B3) exhibited relatively good slag detachability, but the slags with

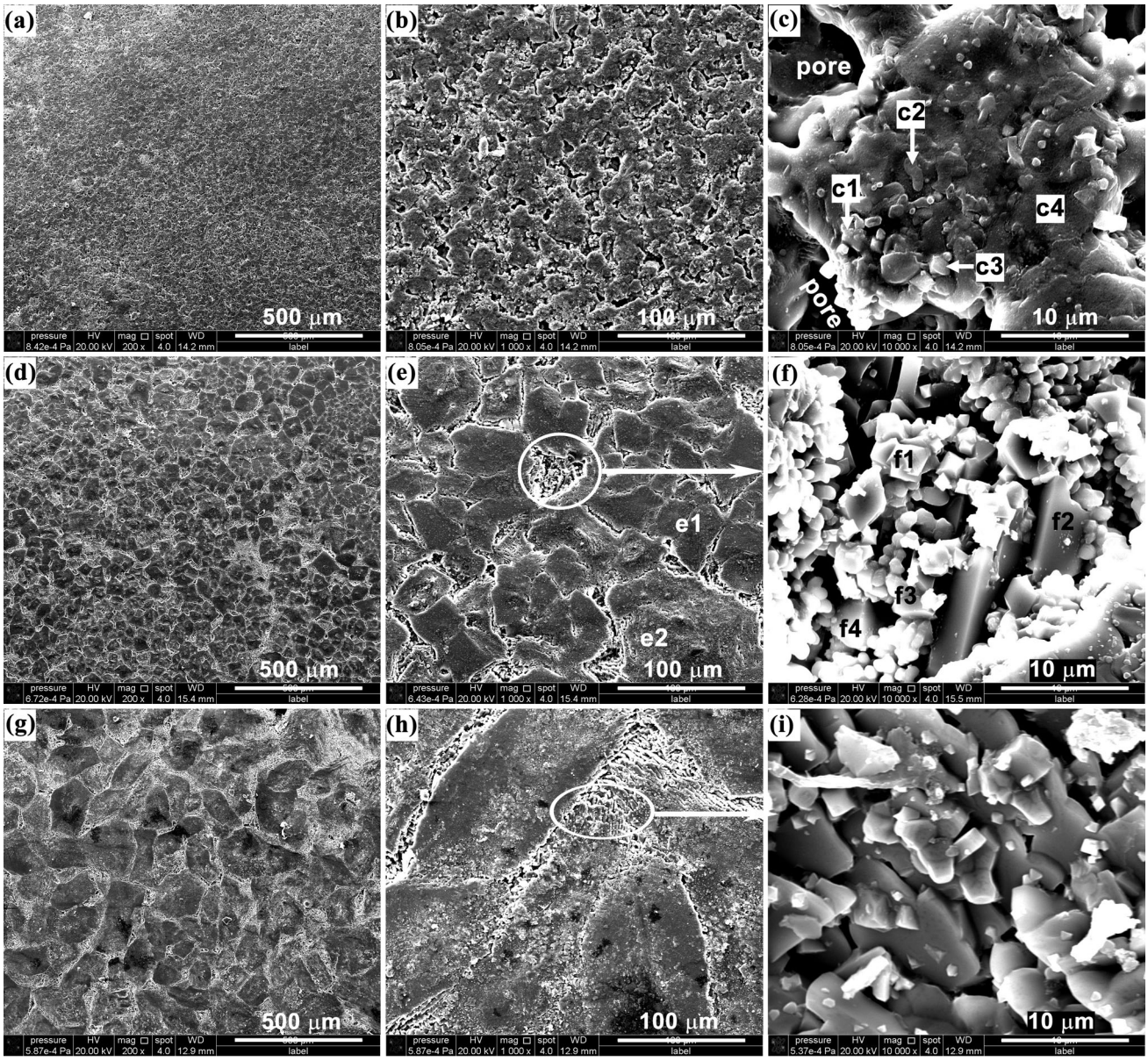

Fig. 7—Microstructures of the A-group slags. (*a*) through (*c*): A1; (*d*) through (*f*): A2; (*g*) through (*i*): A3.

Table V. The Chemical Compositions of the Phases Indicated in Fig. 7c, e, and f (At. Pct)

Phase	O	F	Ca	Si	Mn	Fe	Cr	Ni	Nb	Ti	Al	Mg	Na	K
c1	63.58	4.29	15.95	7.24	1.14	—	—	—	—	0.73	0.35	—	6.45	0.26
c2	25.37	41.15	21.77	4.66	2.56	0.07	0.43	—	—	1.46	0.48	—	2.03	—
c3	50.08	3.05	28.25	10.70	2.67	0.25	—	—	—	1.61	0.75	0.54	2.10	—
c4	56.97	5.74	18.78	6.75	5.19	–	0.56	—	—	2.95	0.93	–	1.70	—
e1	47.66	20.04	16.84	11.15	1.06	0.02	0.47	—	—	0.69	0.35	0.34	1.38	—
e2	45.54	22.40	14.53	10.34	1.41	—	1.16	—	—	0.72	0.67	–	2.86	—
f1	53.63	10.91	3.77	2.66	8.06	0.40	15.98	0.57	—	1.12	0.57	0.88	1.44	—
f2	47.54	11.23	25.72	12.47	1.36	0.13	—	—	—	0.80	—	—	0.76	—
f3	11.12	66.77	15.19	1.23	1.19	0.08	0.96	—	–	0.34	0.27	—	2.86	—
f4	40.93	23.04	17.65	7.63	1.36	0.11	—	—	3.63	1.39	0.65	—	3.61	—

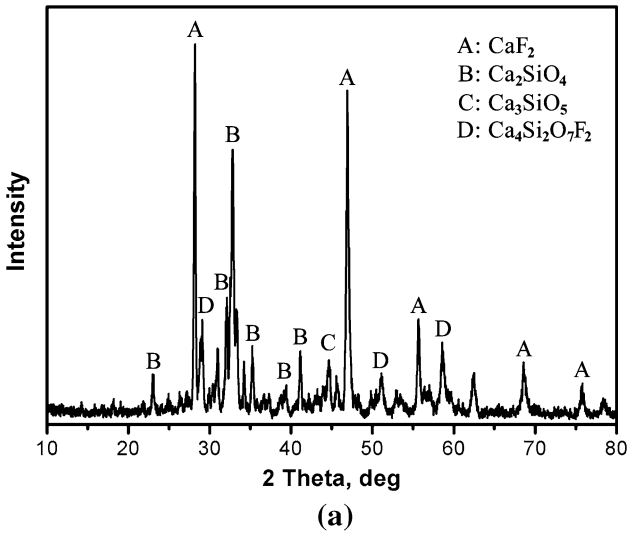

(a)

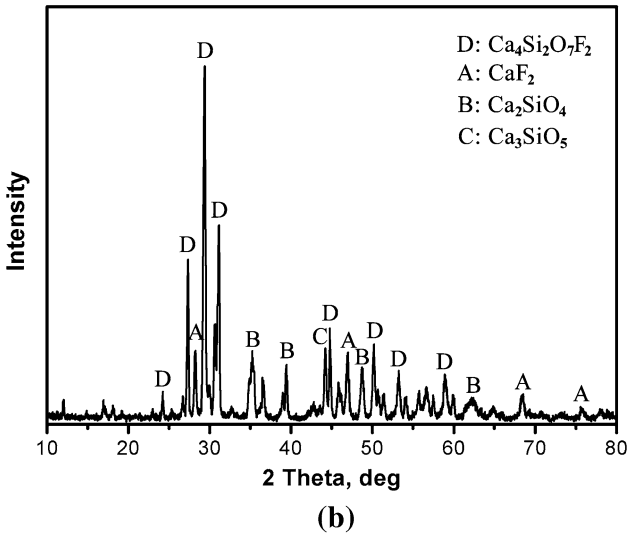

(b)

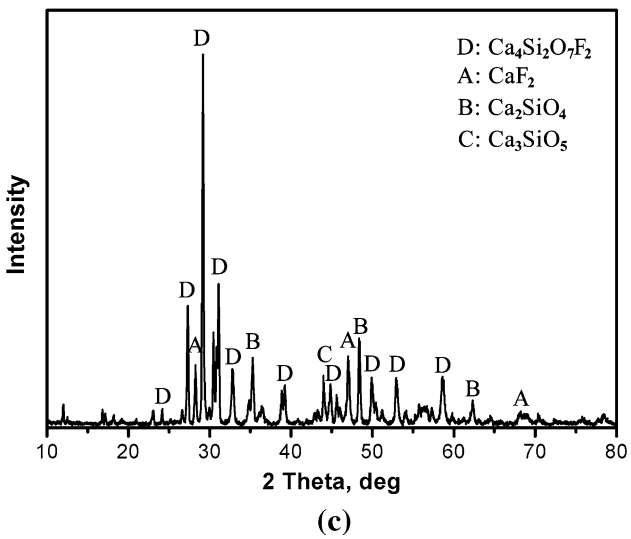

(c)

Fig. 8—XRD patterns taken from the A-group slags. (*a*) A1, (*b*) A2, and (*c*) A3.

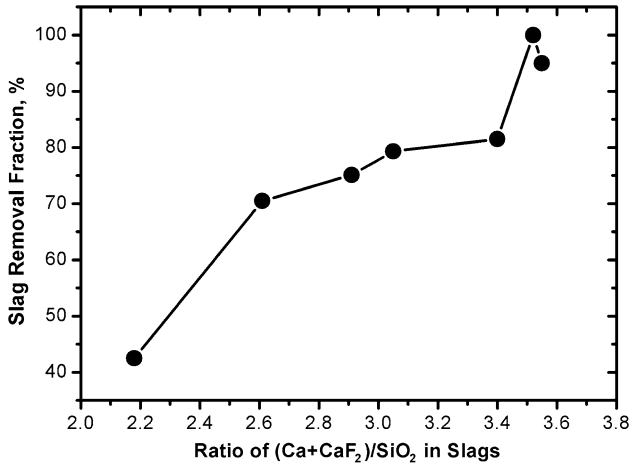

Fig. 9—Effect of the $(CaO + CaF_2)/SiO_2$ ratios in the slags on the slag removal fractions.

smaller thermal expansion coefficients (A2 and A3) had poor slag detachability. In order to more intuitively show the relationship between the three main components and slag detachability, they were plotted in a diagram of the $CaO\text{-}CaF_2\text{-}SiO_2$ ternary system as shown in Figure 11.

It should be mentioned that the mixture of CaO, CaF_2, and SiO_2 tended to gather together forming more complex compounds: $2CaO{\cdot}SiO_2$, $3CaO{\cdot}SiO_2$ and $3CaO{\cdot}2SiO_2{\cdot}CaF_2$ during SMAW due to the free-energy difference[24] as shown in Figure 8. The thermophysical properties (*i.e.*, melting point, thermal expansion coefficient, *etc.*) of the produced compounds are different with that of the single oxide or fluorite.[14,15,24] Among them, the cuspidine ($3CaO{\cdot}2SiO_2{\cdot}CaF_2$) has the lowest melting point [1680 K (1407 °C)],[14] which solidified at the late stage of the slag solidification during SMAW, forming intergranular faceted phases as shown in Figures 7(d) through (i). Such porous phases were brittle, and their broken fine powders were easily embedded in the weld ripples as shown in Figures 1 and 3. According to the $3CaO{\cdot}2SiO_2\text{-}CaF_2$ binary phase diagram,[14] more CaF_2 in the $CaO\text{-}CaF_2\text{-}SiO_2$ slag system led to form the primary solidified CaF_2 and the 'eutectic' cuspidine phase. As the CaF_2 increased, the primary solidified CaF_2 became dominant in the slag, thus strengthening the slag. Such slags had proper strength and tended to detach from the weld metal in large chunks, exhibiting good slag detachability. This case could be found in Al and B3 slags as shown in Figures 1 through 4.

In this study, only the CaO, CaF_2, and SiO_2 were considered because of two reasons. (1) Other oxides such as MnO, Cr_2O_3, Na_2O, Nb_2O_5, and TiO_2 in the slags accounted for small proportion, thus their effects were relatively small. Ignoring their influences could simplify the problem. (2) These oxides could be classified into two categories: acidic and basic oxides. Their

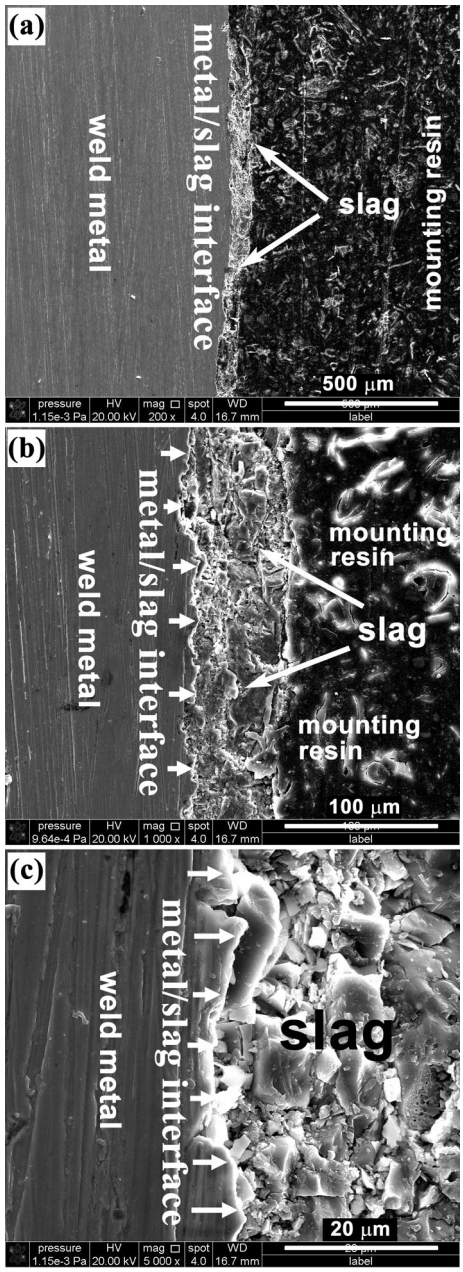

Fig. 10—Images of the weld metal/slag interface of the A3 slag showing the zigzag metal/slag boundary (the magnification increases from (*a*) to (*c*)).

behaviors during SMAW and effects on the slag detachability could be roughly considered to be analogous to that of the SiO_2 or CaO.

Besides, the welding parameters should also affect the welding metallurgical reactions, thus influence the slag composition. It was known that the silicon in the flux would transfer more into the deposited metal as the heat input increased,[11] resulting in less silicon dioxide in the slag. This must affect the slag detachability. The actual effect of the heat input needs a special experimental study.

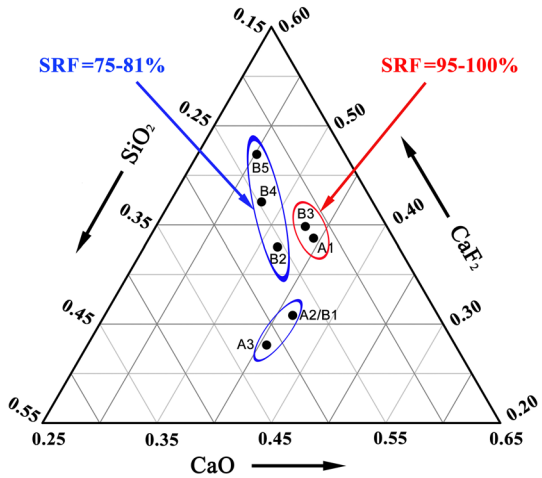

Fig. 11—The slag compositions marked in the CaO-CaF_2-SiO_2 ternary system, showing the dependence of the slag removal fractions on the slag compositions.

V. CONCLUSION

The CaO-CaF_2-SiO_2 type ENiCrFe-7-covered electrodes have been comprehensively investigated in terms of the slag behaviors during SMAW and the slag detachability. The following conclusions can be drawn:

1. Besides the Si being transferred into the weld metal, The SiO_2 in the flux coating interacted with CaF_2 during SMAW to form gaseous SiF_4 to be evacuated. In the reactions, one SiO_2 consumed two CaF_2, leading to the reduction of the ratio of CaF_2/SiO_2. In addition, the CaF_2 was also consumed by reacting with crystal water in the minerals or with moisture pickup from the air at the arc temperature. However, the CaO decomposed from $CaCO_3$ was kept at a relatively constant amount, and almost all were transferred into the slag.
2. The slag detachability could be improved as the SiO_2 in the flux coatings decreased. When the SiO_2 is 10.9 pct, about 28.3 pct CaF_2 resulted in the best slag detachability. In addition, the color of the slags revealed its relation to the slag detachability. The dark blue slag corresponded to the good slag detachability; as the slag color changed from dark blue to deep brown and light brown, the slag detachability tended to deteriorate.
3. The slags were composed of about 80 to 85 pct CaO, CaF_2, and SiO_2, and about 15 to 20 pct Na_2O, MnO, Cr_2O_3, Nb_2O_5, TiO_2, *etc*. If simply considering the slag compositions, the best slag detachability was obtained at CaO:CaF_2:SiO_2 = 1.7:1.8:1, but the worst slag detachability appeared at CaO:CaF_2:SiO_2 = 1.3:0.9:1.
4. The oxides and fluorides in the slags preferred to gather together to form cuspidine and high melting point $2CaO{\cdot}SiO_2$ and $3CaO{\cdot}SiO_2$ phases. If there were more CaF_2 in the slags, they tended to form homogenous porous microstructures composed of

the CaF_2 and the cuspidine. Such slags were relatively strong and would most likely detach from the weld metal in blocks, exhibiting good slag detachability. If there were relatively low CaF_2 in the slags, the cuspidine phase was dominant, leading to form a 'rock strata'-like microstructure in the intergranular area. In this case, the slags were very fragile and could be broken into fine powders that were easily embedded in the weld ripples, leading to slag adhesions.

REFERENCES

1. J.N. DuPont, J.C. Lippold, and S.D. Kiser: *Welding Metallurgy and Weldability of Nickel-Base Alloys*, 1st ed., Wiley, Hoboken, NJ, 2009, pp. 1–5.
2. AWS A5.11/A5.11M: *Nickel and Nickel-Alloy Welding Electrodes for Shielded Metal Arc Welding*, American Welding Society, Miami, FL, 2005.
3. S.D. Strauss: *Power*, 1996, vol. 140, pp. 29–30.
4. D.L. Olson, S. Liu, R.H. Frost, G.R. Edwards, and D.A. Fleming: *Nature and Behavior of Fluxes Used for Welding*, ASM Handbook, Materials Park, OH, 1993, vol. 6, pp. 43–54.
5. C.A. Natalie, D.L. Olson, and M. Blander: *Ann. Rev. Mater. Sci.*, 1986, vol. 16, pp. 389–413.
6. SI Moravetsky: *Paton. Weld. J.*, 2011, vol. 1, pp. 28–31.
7. SI Moravetsky: *Paton. Weld. J.*, 2011, vol. 2, pp. 20–23.
8. K Sham and S Liu: *Welding Journal*, 2014, vol. 8, pp. 271s–81s.
9. D.L. Olson, G.R. Edwards, and S.K. Marya: *Ferr. Alloy Weldments*, 1992, vols. 67–70, pp. 253–68.
10. B. Singh, Z.A. Khan, and A.N. Siddiquee: *J. Mech. Eng. Res.*, 2013, vol. 5, pp. 123–27.
11. R. Qin and G. He: *Metall. Mater. Trans. A*, 2013, vol. 44A, pp. 1475–84.
12. E. Baune, C. Bonnet, and S. Liu: *Weld. J.*, 2000, vol. 79 (3), pp. 57s–65s.
13. H. Nanto, R. Nakagawa, T. Yanagida, Y. Fujimoto, K. Fukuda, Y. Miyamoto, K. Hirasawa, and Y. Takei: *Sens. Mater.*, 2015, vol. 27, pp. 277–82.
14. T. Watanabe, H. Fukuyama, M. Susa, and K. Nagata: *Metall. Mater. Trans. B*, 2000, vol. 31B, pp. 1273–82.
15. B.K. Das, U.S. Yadav, and D.N. Jena: Recycling of steel plant waste through sinter. In: *Proceedings of the national seminar on recent techniques in mineral processing waste and environment management*. by G.V. Rao ed., Indian Institute of Mineral Engineers. Allied Publishers LTD, New Delhi, 2000, pp.187–92.
16. Y. Nakajima and M. Mukai: *ISIJ Int.*, 1993, vol. 33, pp. 109–15.
17. S. Nakamura, F. Tsukihashi, and N. Sano: *ISIJ Int.*, 1993, vol. 33, pp. 53–58.
18. Z. Duan, R. Qin, and G. He: *Metall. Mater. Trans. A*, 2014, vol. 45A, pp. 843–53.
19. J.R. Davis: *ASM Specialty Handbook: Nickel, Cobalt, and Their Alloys*, Materials Park, OH, ASM International, 2000, p. 33.
20. M.D. Almeida, R.J. Brook, and T.G. Carruthers: *J. Mater. Sci.*, 1979, vol. 14, pp. 2191–94.
21. G. Fiquet, P. Richet, and G. Montagnac: *Phys. Chem. Minerals*, 1999, vol. 27, pp. 103–11.
22. B. Schumann and H. Neumann: *Crystal Res. Technol.*, 1984, vol. 19, pp. K13–K14.
23. M. Amri, G.J. Clarkson, and R.I. Walton: *J. Phys. Chem. C*, 2010, vol. 114, pp. 6726–33.
24. T. Watanabe, H. Fukuyama, and K. Nagata: *ISIJ Int.*, 2002, vol. 42, pp. 489–97.